Solid solubility and photoluminescence of $Y_3Al_5O_{12}:Ce^{3+}$ prepared by using $(Y_{1-x}Ce_x)_2O_3$ as precursor*

Liu Si-Jia(刘思佳)[a], Peng Tong-Jiang(彭同江)[a], Song Zhen(宋 振)[b], Bian Liu(边 柳)[b], Song Gong-Bao(宋功保)[a], and Liu Quan-Lin(刘泉林)[b]†

[a] School of Materials Science & Engineering, Southwest University of Science and Technology, Mianyang 621010, China
[b] School of Materials Science & Engineering and State Key Laboratory for Advanced Metals and Materials, University of Science and Technology Beijing, Beijing 100083, China

(Received 27 September 2013; revised manuscript received 16 December 2013; published online 20 February 2014)

Trivalent cerium-doped yttrium aluminum garnet (YAG:Ce^{3+}) phosphors are synthesized by solid-state reaction method through using $(Y_{1-x}Ce_x)_2O_3$ solid solutions as precursors. Solid solubility limits of Ce^{3+} replacing Y^{3+} in Y_2O_3 and YAG are determined to be 40% and 7.5%, respectively, based on the relationship between the lattice parameter and chemical composition. Using $(Y_{1-x}Ce_x)_2O_3$ as precursors we synthesize YAG:Ce^{3+} single phase at 1450 °C and N_2 atmosphere. However, under the same conditions using CeO_2 there exists a second phase $YAlO_3$ as impurity. The photoluminescence intensity of YAG:Ce^{3+} increases monotonically with the increase of Ce concentration until it reaches a maximum at solid solubility limits of Ce^{3+} in YAG.

Keywords: luminescence, YAG, solid solubility, LED

PACS: 81.20.–n, 78.55.Hx, 61.55.Fn **DOI:** 10.1088/1674-1056/23/4/048106

1. Introduction

The white light emitting diodes (WLEDs) are proliferating all over the world and are increasingly replacing conventional light sources, such as incandescent or fluorescent lamps, because of their energy-saving, long lifetime, compactness, and environmental friendliness.[1–5] A typical commercially available WLED features a combination of blue InGaN chips with yttrium aluminum garnet $Y_3Al_5O_{12}:Ce^{3+}$ (YAG:Ce) phosphor, in which the phosphor strongly absorbs blue light from the LED chip and efficiently re-emits in the yellow part of the visible spectrum.[6–8] The combination of the yellow YAG:Ce emission and blue radiation bleeding through the phosphor coating (on top of a blue LED) gives white light. Since the quality of phosphors is vital to the performance of a WLED device, the quest for further improving properties of YAG:Ce phosphor is very important and a significant challenge.

YAG, i.e., $\{Y\}_3[Al]_2(Al)_3O_{12}$, has a garnet-type structure, generally denoted as $\{A\}_3[C]_2(D)_3O_{12}$, where the $\{A\}$ cations are eight-coordinated in dodecahedra, the [C] cations are octahedrally coordinated, and the (D) tetrahedrally coordinated.[9] The luminescence of cerium-doped YAG was first reported in 1967, which shows a yellow emission band from the allowed 5d→4f transition (to the spin–orbit split $^2F_{7/2}$ and $^2F_{5/2}$ levels).[10,11] Gd^{3+} substitution for the $\{Y\}$ sites can move the YAG:Ce emission band to red region, while Ga^{3+} replacement for [Al] or (Al) sites or Lu substitution on $\{Y\}$ sites can cause a blue shift.[12–14]

Besides the qualified spectral properties, the commercial YAG:Ce phosphor for WLED requires other qualities, such as high luminescent intensity, good powder mobility, well-shaped crystal form, and uniform size distribution, which are dependent on the synthesis approach. Several methods have been reported to synthesize YAG:Ce phosphors. High-temperature solid-state reaction is the most common method to synthesize YAG:Ce phosphors. Other preparations, such as solvothermal synthesis,[15] sol–gel method,[16] co-precipitation method,[17] sol–gel combustion,[18] metal–organic chemical vapor deposition (MOCVD),[19] and spark-plasma synthesis,[20] are also used to synthesize nano YAG:Ce phosphors. Generally nano particles are poorly crystallized and have huge specific surface areas, which results in low luminescent intensity and severe agglomeration even after calcination. Ball shaped particles can be obtained by spray pyrolysis method.[21] Moreover, YAG has been successfully manufactured by some modified methods like a liquid-to-particle conversion process, usually known as the gel supported precipitation (GSP) method[22] and a modified sol–gel method using poly (ethylene glycol) (PEG) and urea.[23] High-temperature solid-state reaction with the help of using appropriate flux can fabricate good YAG:Ce phosphor with high lu-

*Project supported by the National Natural Science Foundation of China (Grant No. 51272027) and the Ph. D. Program Foundation of Education Ministry of China (Grant No. 20100006110011).

†Corresponding author. E-mail: qlliu@ustb.edu.cn

© 2014 Chinese Physical Society and IOP Publishing Ltd

minescent intensity and well-shaped crystal form and uniform size distribution.[24]

Ce^{3+} ions have a limited solid solubility in YAG, depending on the synthesis conditions. Since Tien *et al.*[13] reported that only 2 mole percent of Ce^{3+} can be dissolved in YAG in air while almost 6% Ce^{3+}enters into the lattice when being fired at 1450 °C under a hydrogen atmosphere, few studies have reported on the Ce solid solubility in YAG. Generally, luminescence intensity of YAG:Ce is related to Ce concentration, uniformity of Ce distribution in lattice, and crystalline quality of YAG:Ce. Usually, CeO_2 is used as Ce source to synthesize the YAG:Ce through the solid state reaction, where Ce^{4+} ions in CeO_2 are needed to reduce Ce^{3+} ions in YAG:Ce. In this work, we first prepare a series of $(Y_{1-x}Ce_x)_2O_3$ solid solutions ($x = 0.05$–0.6) containing Ce^{3+}, then we use them as precursors to synthesize YAG:Ce phosphors in order to guarantee that valence of Ce ions is +3 and increase their solid solubility in YAG. Furthermore, we determine the Ce solid solubility in YAG and investigate its luminescence.

2. Experiment

Solid solutions $(Y_{1-x}Ce_x)_2O_3$ and $Ce_xY_{1-x}O_2$ were prepared via precipitation using ammonium hydrogen carbonate (NH_4HCO_3, analytical purity) as the precipitant. The starting salts were cerium and yttrium nitrate hexahydrates ($RE(NO_3)_3{\cdot}6H_2O$, RE = Ce and Y) with a purity of higher than 99.99%. All the chemical materials were used without further purification. The stock solutions were made by dissolving the cerium and yttrium salts into distilled water. To make sure that Ce^{3+} and Y^{3+} cations were fully mixed at the predetermined molar ratio, the final concentration of each stock solution was 0.015 M for Y^{3+} plus Ce^{3+} cations. Aqueous solutions of ammonium hydrogen carbonate with a concentration of 0.075 M were used as the precipitant. In a typical synthetic procedure, the 50-cm^3 mixed salt solution was dripped at a speed of 2.5 $cm^3{\cdot}min^{-1}$ into 75 cm^3 of the precipitant solution that was kept at 30° under mild stirring. The resulting suspension, after having been homogenized for 20 min, was filtered via suction filtration. The precipitate cake was washed repeatedly with distilled water and finally rinsed with anhydrous alcohol (except those for chemical analysis) before drying at 90 °C in an electricity heat drum wind drying oven. The dried precursor was lightly crushed with a silica mortar and pestle and then calcined in a box-type furnace at 1200 °C for 1.5 h to yield oxide powders.

Powder samples of $(Y_{1-z}Ce_z)_3Al_5O_{12}$ were synthesized by conventional high-temperature solid-state reaction. Stoichiometric amounts of raw material γ-Al_2O_3 and $(Y_{1-x}Ce_x)_2O_3$ solid solution prepared as above were thoroughly mixed and grounded in an agate mortar. Then the mixture was pressed into pellets and sintered in a vacuum annealing furnace under 10% H_2/90% N_2 (V/V) atmosphere at 1550 °C for 2 h. Finally, the samples were cooled down to room temperature in the reducing atmosphere. The synthesized phosphors were ground into powder for further study.

The X-ray diffraction (XRD) data were collected on a Rigaku D max A diffractometer (40 kV×35 mA) with Cu $K_{\alpha1}$ radiation ($\lambda = 0.15406$ nm). Continuous scan mode with a 2θ scan range of 15 °–75° was employed. The lattice parameter data were taken on XRD data by the Rietveld refinement method through using program FullProf for $(Y_{1-x}Ce_x)_2O_3$ and $Ce_xY_{1-x}O_2$ precursors or by least square method for $(Y_{1-z}Ce_z)_3Al_5O_{12}$ based on internal standard method through using crystalline silicon as internal standard. The photoluminescence (PL) spectra were collected with an Edinburgh Instruments FLS920 equipped with a continuous (450 W) xenon lamp. Slit width of 0.3 nm was used on the excitation and emission monochromators. The step width was 1.0 nm and the dwell time was 0.20 s. The line intensities and positions of the measured spectra were corrected by the FLS920 correction curve. JEOL JSM-6510A microscope was employed to take SEM photos of samples.

3. Result and discussion

The X-ray diffraction (XRD) patterns of some representative $(Y_2O_3)_{1-x}(CeO_2)_x$ compositions ($x = 0.1$, 0.4, 0.5, 0.55, 0.6, 0.7, and 0.95) in a range of 15°–75° are shown in Fig. 1. When $0.0 \leq x \leq 0.4$, the XRD patterns match well with the reported pattern of Y_2O_3 phase with the body-centered cubic lattice (ICCD 04-005-5119, space group $Ia3$), herein represented as $(Y_{1-x}Ce_x)_2O_3$, which reveals that the Ce^{3+} ions successfully substitute for the Y^{3+} ions in Y_2O_3 structure. For the samples with $0.6 \leq x \leq 1.0$, the XRD patterns representing a cubic fluorite structure phase CeO_2 (ICCD 00-004-0593, space group $Fm3m$), denoted as $Ce_xY_{1-x}O_2$, are observed. The compositions with $0.5 \leq x \leq 0.55$ have two phases, i.e., $Ce_xY_{1-x}O_2$ phase with fluorite structure and $(Y_{1-x}Ce_x)_2O_3$ phase with body-centered cubic structure. The idealized body-centered cubic structure of Y_2O_3 is a fluorite-derived structure with space group $Ia3$; its lattice parameter a ($\sim$ 10.603 Å) is about twice as long as that of CeO_2 with fluorite structure ($\sim$ 5.411 Å).[25,26] Therefore, the fundamental reflections of the two phases are almost the same, except that there exist some weak super-structure peaks in addition to the fundamental reflections for the XRD patterns of CeO_2 phase.[27] With the Ce content in Y_2O_3 increasing, these super-peaks become

weaker and weaker until they disappear at $x = 0.55$.

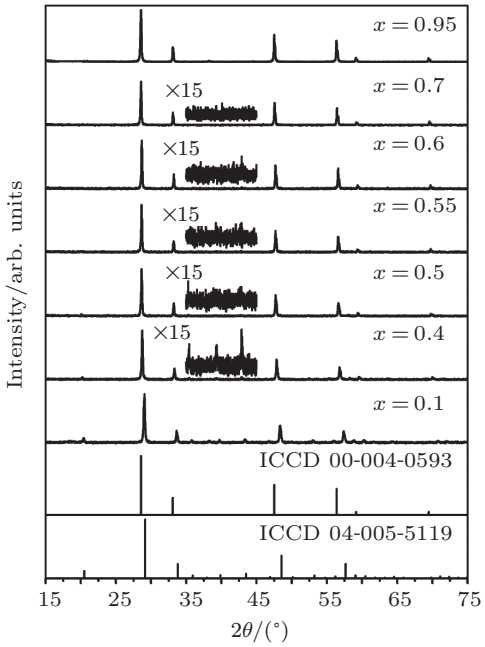


Fig. 1. The XRD patterns of some representative $(Y_2O_3)_{1-x}$ $(CeO_2)_x$ compositions ($x = 0.1$, 0.4, 0.5, 0.55, 0.6, 0.7, and 0.95).

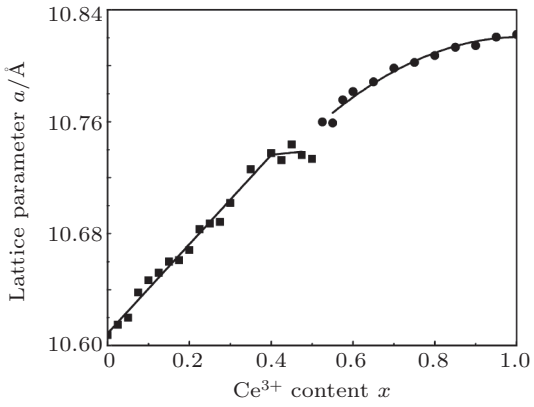


Fig. 2. Lattice parameters a of $(Y_{1-x}Ce_x)_2O_3$ ($0 \le x < 0.55$) and double lattice parameters a of $Ce_xY_{1-x}O_2$ ($0.55 \le x \le 1$) versus Ce^{3+} content, where solid square (■) represents the lattice parameters of $(Y_{1-x}Ce_x)_2O_3$ phase with body-centered cubic structure and solid circle (•) denotes double lattice parameters of $Ce_xY_{1-x}O_2$ phase with fluorite structure for clear comparison (the actual lattice parameters range from 5.3902 Å to 5.4111 Å).

Figure 2 shows the relation between the lattice parameters a of $(Y_{1-x}Ce_x)_2O_3$ ($0 \le x < 0.55$) and double lattice parameters a of $Ce_xY_{1-x}O_2$ ($0.55 \le x \le 1$) and Ce^{3+}concentration ($x = 0$–1.00). For clear comparison, we double the lattice parameters of $CexY_{1-x}O_2$ phase (the actual lattice parameters range from 5.3902 Å to 5.4111 Å) since the structures of Y_2O_3 and CeO_2 both are closely related to the fluorite-type structure. The lattice parameters of $(Y_{1-x}Ce_x)_2O_3$ increase linearly with the increase of Ce^{3+} concentration when $x \le 0.4$, which is in reasonable agreement with Vegard's law with the ionic radius of Ce^{3+} ($r = 0.101$ nm, C. N. = 6) larger than that of Y^{3+} ($r = 0.090$ nm, C. N. = 6). This increasing linear relation confirms that it is Ce^{3+} ion not Ce^{4+} ion that has successfully substituted for Y^{3+} ion in the lattice, since the ionic radius of Ce^{4+} ($r = 0.087$ nm, C. N. = 6) is smaller than that of Y^{3+}. In the range of $0.6 \le x \le 1.0$, the lattice parameters increase parabolically (not linearly) with the increase of Ce^{3+} concentration in $Ce_xY_{1-x}O_2$, because there exist anion (oxygen) vacancies in CeO_2 structure for maintaining charge balance where the valence of Ce ion is +4 and the valence of Y ion is +3.[25] When $0.4 < x < 0.6$, there is a discontinuity in the linear relationship between the lattice constant and chemical compositions, indicating that the two phases $(Y_{1-x}Ce_x)_2O_3$ and $Ce_xY_{1-x}O_2$ co-exist.

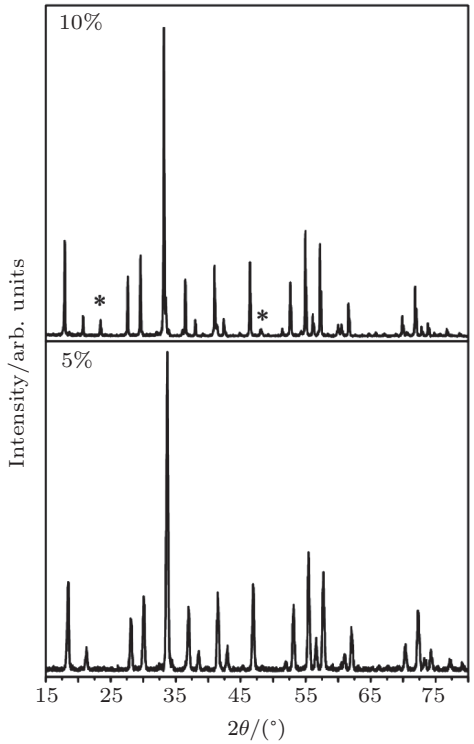


Fig. 3. Typical XRD patterns of the sample $(Y_{1-z}Ce_z)_3Al_5O_{12}$ with $z = 0.05$ and 0.10. $*$ denotes $CeAlO_3$ phase.

The typical X-ray diffraction patterns of the sample $(Y_{1-z}Ce_z)_3Al_5O_{12}$ with $z = 0.05$ and 0.10 are shown in Fig. 3. With the lower Ce^{3+} concentration, single phase YAG:Ce is obtained, which accords with the patterns of YAG (ICCD 04-007-2667, cubic, space group *Ia*3*d*) with a garnet structure. For the sample with $z = 0.1$, some impurity phases such as $CeAlO_3$ (ICCD 00-055-0890) are observed in the phosphors. In order to obtain the solid solubility of Ce^{3+} in YAG, the lattice constants of $(Y_{1-z}Ce_z)_3Al_5O_{12}$ ($z = 0$–0.2) are calculated based on the XRD patterns with Si as internal standard and they are depicted to vary with Ce^{3+} concentration in Fig. 4. As mentioned above, in $(Y_{1-x}Ce_x)_2O_3$ solid solutions ($x \le 0.4$) the lattice constants are linearly dependent on Ce^{3+} concentration. While in the YAG phases which were synthesized by

conventional high-temperature solid state reaction through using raw material γ-Al_2O_3 and $(Y_{1-x}Ce_x)_2O_3$ solid solutions as precursors, the lattice constants are linearly increasing with Ce^{3+} concentration only in the range of $0 \leq z \leq 0.075$, then stays at a relatively stable value when $z > 0.075$. This reveals that the solid solution limit of Ce^{3+} ions in YAG is about 7.5%, which is a little larger than that (the solid-solution limit is 6%) reported by Tien *et al.*[13]

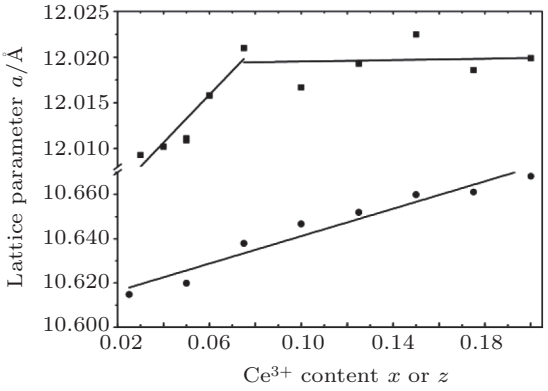


Fig. 4. Curves of the lattice constants of $(Y_{1-z}Ce_z)_3Al_5O_{12}$ (■) and $(Y_{1-x}Ce_x)_2O_3$ (●) versus Ce^{3+} concentration. The data of $(Y_{1-x}Ce_x)_2O_3$ which are the same as those in Fig. 2 are re-plotted here for better comparison.

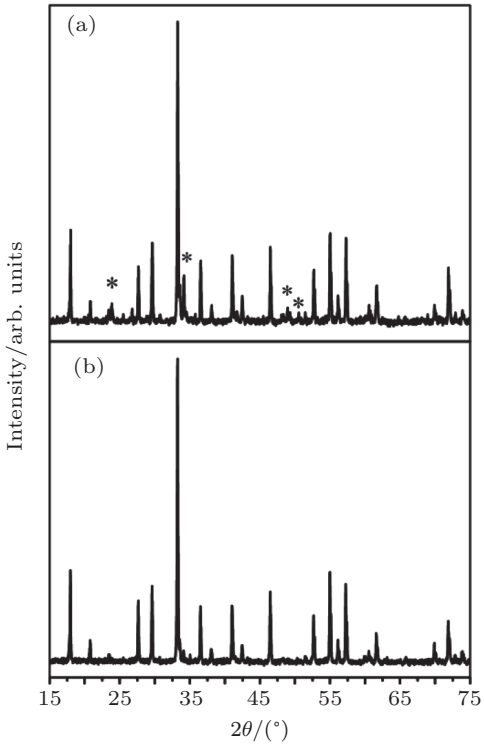


Fig. 5. XRD patterns of $(Y_{0.95}Ce_{0.05})_3Al_5O_{12}$ prepared by solid-state reaction (sintered at 1450 °C under N_2 flow for 2 h) using different raw materials: (a) direct mixture Y_2O_3, CeO_2, and γ-Al_2O_3; (b) $(Y_{0.95}Ce_{0.05})_2O_3$ and γ-Al_2O_3. $*$ indicates $YAlO_3$ phase.

In comparison with the conventional solid-state reaction, the route to synthesizing YAG:Ce pure phase by using $(Y_{0.95}Ce_{0.05})_2O_3$ solid solutions as precursors needs a lower temperature. As shown in Fig. 5, the sample synthetized by using $(Y_{0.95}Ce_{0.05})_2O_3$ as precursor is pure YAG:Ce phase, while the sample prepared by the conventional method contains YAG:Ce and $YAlO_3$ phases (at 1450 °C under N_2 atmosphere without any flux). Because we have dispersed Ce ions fully in the lattice Y_2O_3 and the nanoparticle-precursors prepared by precipitation is in favor of the solid-state reaction, we can synthesize YAG:Ce pure phase at lower temperature (1450 °C) and under weakly reduced condition (solely using N_2 not N_2/H_2).

Figure 6 shows representative SEM images of the samples of $(Y_{1-x}Ce_x)_2O_3$ with $x = 0.05$ and $(Y_{1-z}Ce_z)_3Al_5O_{12}$ with $z = 0.05$. The particles of the solid solution $(Y_{0.95}Ce_{0.05})_2O_3$ synthesized by precipitation method are basically spherical in shape and dispersed well as shown in Fig. 6(a). The average size of particles is on a nano scale. This spherical and nanoscale-sized precursor can provide more contact between reactants to drive the subsequent solid-state reaction. The phosphors $(Y_{0.95}Ce_{0.05})_3Al_5O_{12}$ obtained by the solid-state reaction method seem to have a tendency to form bigger particles of around 2 μm in size as shown in Fig. 6(b).

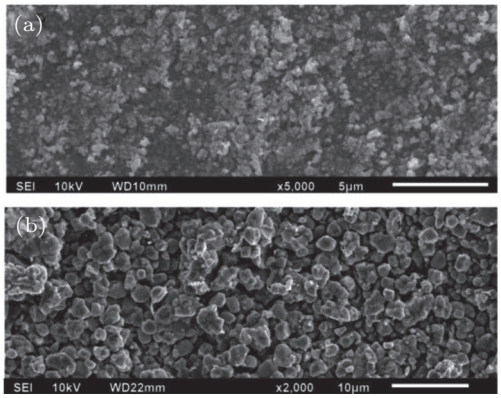


Fig. 6. Representative SEM images of the samples of $(Y_{1-x}Ce_x)_2O_3$ with $x = 0.05$ (a) and $(Y_{1-z}Ce_z)_3Al_5O_{12}$ with $z = 0.05$ (b).

The PL spectra of the YAG:Ce phosphors are measured at room temperature as a function of the activator concentration. Figures 7(a) and 7(b) show the 450-nm-excited emission spectra and excitation spectra of the YAG:Ce phosphors with different Ce concentrations calcined at 1550 °C for 2 h, respectively. It can be noticed that both the shapes and positions of the excitation spectra show no obvious changes with the increase of Ce concentration. The excitation spectra for Ce^{3+} contain two bands, namely, a weak band with a maximum at 349 nm and a strong broad band ranging from 400 nm to 500 nm with a maximum at 450 nm, which is very suitable for serving as a color converter in white LED excited by a commercial InGaN blue LED. These excitation bands are due to the absorption of the incident radiation by Ce^{3+} ion which

leads to the excitation of electrons from the $4f^1$ ground state ($^2F_{5/2}$, $^2F_{7/2}$) to the excited $5d^1$ levels (^2D).[28] The emission of Ce^{3+} is ascribed to the electron transition from the lowest crystal-splitting component of 5d level to the ground state of Ce^{3+} ($^2F_{5/2}$, $^2F_{7/2}$). It is also noticed that all the emission peaks have maximum intensity at about 550 nm. The PL intensities of the YAG:Ce phosphors increase with the Ce concentration increasing without the concentration quenching effect until they reach a maximum value 5.448×10^8 (integral intensity) at $z = 0.075$, which is also the Ce solid-solubility limit in YAG structure.[29] The luminescent intensity is influenced by the average distance between luminescent centers. As the doping concentration increases, the separation between active ions decreases. At short enough separation the interaction between active ions will occur and cause concentration quenching.[30] Therefore, the homogeneous distribution of active ions in host is essential in order to acquire highly efficient phosphors without concentration quenching. Our results that PL intensities of the YAG:Ce phosphors increase with the Ce content until solid-solubility limit, indicate that the homogeneous distribution of Ce ions in YAG host can be obtained by using $(Y_{1-x}Ce_x)_2O_3$ solid solutions as precursors.

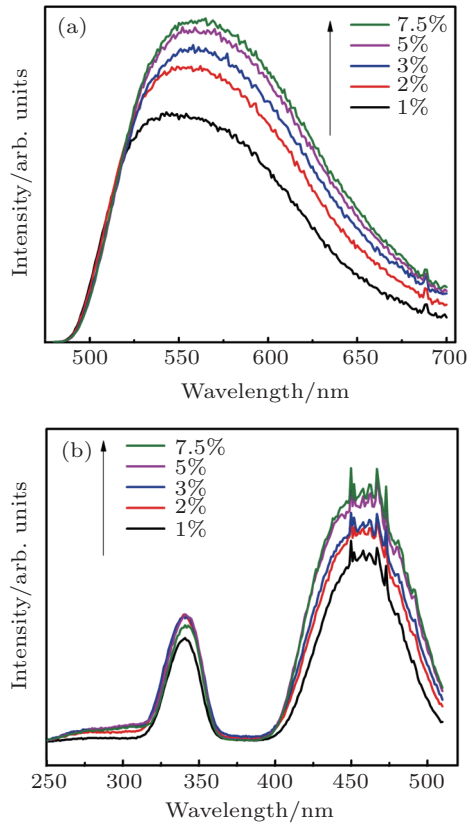


Fig. 7. (color online) The PL emission spectra with $\lambda_{ex} = 450$ nm (a) and excitation spectra with $\lambda_{em} = 550$ nm (b) of $(Y_{1-z}Ce_z)_3Al_5O_{12}$ phosphors for the cases of various Ce concentrations

4. Conclusion

In this paper, we successfully synthesized YAG:Ce^{3+} phosphors by solid-state reaction method through using $(Y_{1-x}Ce_x)_2O_3$ solid solutions as precursors. According to the relationship between the lattice parameter and chemical composition, solid solubility limits of Ce^{3+} replacing Y^{3+} in Y_2O_3 and YAG are determined to be 40% and 7.5%, respectively. It is easier to synthesize pure YAG:Ce^{3+} phase by solid-state reaction through using $(Y_{1-x}Ce_x)_2O_3$ as precursors than through using CeO_2. Photoluminescence intensity of YAG:Ce^{3+} increases monotonically with Ce-doped content increasing until it reaches a maximum at solid solubility limit of Ce^{3+} in YAG, i.e. $\sim 7.5\%$.

References

[1] Malakoff D 2002 *Science* **296** 1782
[2] Xiao H Y, Xia Z G, Liao L B, Zhou J and Zhuang J Q 2012 *J. Alloys Compd.* **534** 97
[3] Zhou T L, Song Z, Song X P, Bian L and Liu Q L 2010 *Chin. Phys. B* **19** 127808
[4] Tian H, Liu J W, Qiu K, Song J and Wang D J 2012 *Chin Phys. B* **21** 098504
[5] Bian L, Wang T, Song Z, Liu Z H, Li J X and Liu Q L 2013 *Chin Phys. B* **22** 077801
[6] Nakamura S and Fasol G 1997 *The Blue Laser Diode: GaN Based Light Emitters and Lasers* (Berlin: Springer)
[7] Nakamura S 2009 *MRS Bull.* **34** 101
[8] Schubert E F and Kim J K 2005 *Science* **308** 1274
[9] Geller S 1967 *Z. Kristallogr. Bd.* **125** 1
[10] Blasse G and Bril A 1967 *Appl. Phys. Lett.* **11** 53-55
[11] Holloway W Jr and Kestigian M 1967 *Phys. Lett. A* **25** 614
[12] Holloway W W and Kestigian M 1969 *J. Opt. Soc. Am.* **59** 60
[13] Tien T, Gibbons E, DeLosh R, Zacmanidis P, Smith D and Stadler H 1973 *J. Electrochem. Soc.* **120** 278
[14] Robertson J M, Van Tol N W, Smits W H and Heynen J P H 1981 *Philips J. Res.* **36** 15
[15] Sang Y, Liu H, Lü Y, Wang J, Chen T, Liu D, Zhang X, Qin H, Wang X and Boughton R I 2010 *J. Alloys Compd.* **490** 459
[16] Fadlalla H M and Tang C C 2009 *J. Crystal Growth* **311** 3737
[17] Pan Y, Wu M and Su Q 2004 *Mater. Sci. Eng.* **106** 251
[18] Li H L, Liu X J and Huang L P 2007 *Opt. Mater.* **29** 1138
[19] Li Y, Zhang J, Xiao Q and Zeng R 2008 *Mater. Lett.* **62** 3787
[20] Suareza M, Fernandez A, Menendez J L and Torrecillas R 2010 *J. Alloys Compd.* **493** 391
[21] Maniquiz M C, Jung K Y and Jeong S M 2011 *J. Electrochem. Soc.* **158** 697
[22] Fernandez A and Somers J 2003 *J. Mater. Sci.* **38** 2331
[23] Ogi T, Nandiyanto A B and Wang W N 2012 *Chem. Eng. J.* **210** 461
[24] Song Z, Liao J, Ding X L, Liu X L and Liu Q L 2013 *J. Crystal Growth* **365** 24
[25] Barker W W and Wilson A F 1968 *J. Inorg. Nucl. Chem.* **39** 1415
[26] McBride J R, Hass K C, Poindexter B D and Weber W H 1994 *Appl. Phys.* **76** 2435
[27] Djurovic D, Zinkevich M and Aldinger F 2008 *Solid State Ionics* **179** 1902
[28] Tachiwaki T and Yoshinaka M 2001 *Solid State Commun.* **119** 603
[29] Liu Y, Zhang Z F, King B, Halloran J and Laine R M 1996 *J. Am. Ceram. Soc.* **79** 385
[30] Yang H, Yuan L, Zhu G, Yu A and Xu H 2009 *Mater. Lett.* **63** 2271